Interference effects between $2p$ photoionization and resonant Auger decay channels at $2s^{-1}np$ $(n=4,5)$ inner-shell resonances in Ar

R. Sankari, A. Kivimäki, M. Huttula, T. Matila, H. Aksela, and S. Aksela
Department of Physical Sciences, University of Oulu, P.O. Box 3000, 90014 University of Oulu, Finland

M. Coreno
Instituto Nazionale per la Fisica de la Materia—Technologie Avanzate di Superficie e Catalisi, I-34012 Trieste, Italy

G. Turri
Instituto Nazionale per la Fisica de la Materia—Technologie Avanzate di Superficie e Catalisi, I-34012 Trieste, Italy and Dipartimento di Fisica, Politecnico di Milano, I-20133 Milano, Italy

R. Camilloni
Consiglio Nazionale delle Ricerche—Instituto di Metodologie Avanzate Inorganiche, Area della Ricerca di Roma, CP-10, I-00016 Rome, Italy

M. de Simone
Dipartimento di Fisica, Università di Roma III, I-00146 Rome, Italy

K. C. Prince
Sincrotrone Trieste, I-34012 Trieste, Italy

(Received 31 October 2001; published 14 March 2002)

The electron spectrum of Ar has been studied in the binding energy region of the $2p^{-1}3p^{-1}np$ states. These states are populated in direct $2p$ photoionization accompanied by the $3p\rightarrow np$ shake-up transitions. In addition, at photon energies corresponding to the $2s\rightarrow 4p,5p$ excitations they gain intensity through the $2s^{-1}np \rightarrow 2p^{-1}3p^{-1}np$ resonant Auger decay channels. The two channels can interfere, leading to changes in the intensities of the Ar $2p$ photoelectron satellites. Experimental results are compared with the results of one-step calculations.

DOI: 10.1103/PhysRevA.65.042702 PACS number(s): 32.80.Hd, 32.80.Fb

I. INTRODUCTION

Direct photoionization and the decay after resonant excitation can populate the same final states. Due to the wave nature of the electrons, the two different channels can interfere. The interference effect between the resonant Auger decay following the inner-shell excitation and the direct photoionization was reported by Camilloni *et al.* [1]. In their study, the photon energy was scanned across the resonance and the variation of the branching ratios of the intensities of the different final states was observed. The same experimental technique was applied in the recent study of Marinho *et al.* [2] and a clear Fano profile was detected in a constant ionic state spectrum of selected final states as a consequence of the two interfering channels. In both studies one-step calculations were not performed although a need for them was clearly expressed.

In the present work the intensity and angular distributions of some of the Ar $2p$ shake-up satellite transitions, namely, to the $2p^{-1}3p^{-1}np$ and $2p^{-1}3p^{-1}ns$ $(n=4,5)$ states, are determined on and off $2s^{-1}4p$ and $2s^{-1}5p$ resonances. At photon energies corresponding to the $2s\rightarrow 4p,5p$ excitations the direct and resonant channels to $2p^{-1}3p^{-1}np$ states have comparable intensities, therefore interference effects are expected to occur. Calculations based on the one-step approximation have been used to explain the detected variation in the intensities of the $2p^{-1}3p^{-1}4p$ states. The states that can be seen in the Ar $2p$ shake-up spectrum were widely studied using conventional x-ray sources [3–6]. Theoretical calculations made in the study of Eriksson *et al.* [6] provided an approximate assignment of the Ar $2p^{-1}3p^{-1}np$ satellite states. More recent Ar $2p$ satellite studies have been made using synchrotron radiation [7,8]. In brief, the states where the interference effects are excpected to occur are well resolved and described by existing theoretical models. On the other hand, the $2s$ core-hole ionization or excitation and subsequent decay have rarely been studied [9–12]. Recently, however, Itchkawitz *et al.* [13] presented a high-resolution absolute photoabsorption cross-section measurement covering the $2p$ and $2s$ edges of argon, whereas Khoperskii and Yavna [14] investigated Ar $2s$ photoabsorption theoretically. The two latter studies provide information about expected strengths of the direct and resonance channels but the decay paths of the excited states were not investigated.

In this study the direct and resonant Auger decay channels to Ar $2p^{-1}3p^{-1}np$ $(n=4,5)$ were investigated in detail. The experimental spectra were compared with the results obtained from the one-step calculations.

II. EXPERIMENT

The measurements were performed at the Gas Phase Photoemission beam line of the ELETTRA storage ring in Trieste, Italy. An undulator source provides high-intensity syn-

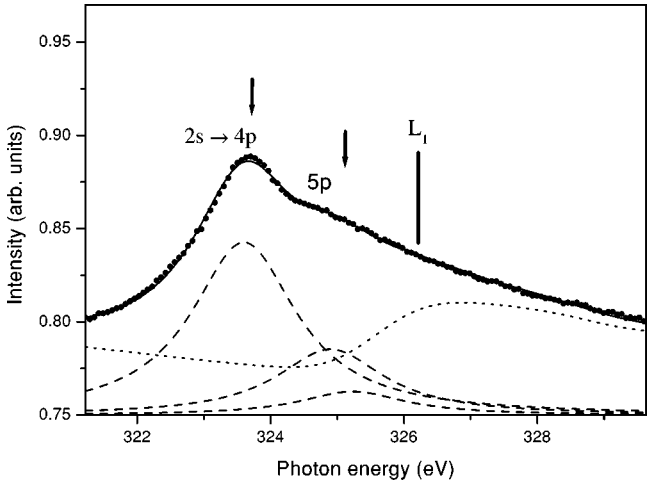

FIG. 1. L_1 pre-edge Rydberg excitations in Ar. Dots show the experimental data, whereas the solid and dashed lines give the least-squares fit for the whole spectrum and individual transitions, respectively. The dotted line describes the contribution of the higher Rydberg excitations and the ionization continuum. The resonant Auger spectra were measured at photon energies marked with arrows. The vertical bar shows the L_1 ionization limit.

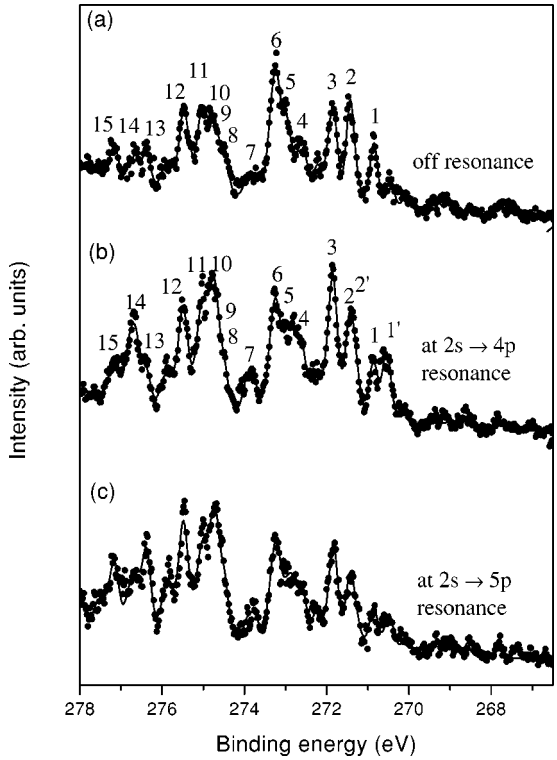

FIG. 2. (a) Ar $2p$ photoelectron shake-up satellite spectrum measured at 310 eV photon energy. The electron spectra of Ar measured at photon energies corresponding to (b) the $2s \rightarrow 4p$ and (c) $2s \rightarrow 5p$ excitations (see Fig. 1). In all panels, dots show the experimental data and the solid lines give the least-squares fit results for the whole spectrum. All the spectra presented were measured at 60° with respect to the electric vector of the incident synchrotron radiation.

chrotron radiation in the photon energy range 20–900 eV. The highly polarized light [15] is dispersed by a variable-angle spherical grating monochromator that is equipped with five interchangeable gratings, fixed entrance and exit slits, and pre- and postfocusing optics. A more detailed description of the beam line can be found elsewhere [16].

The experimental setup for the total ion yield and angle-resolved electron spectra has been presented earlier [15,17]. For the resonant Auger measurements, the photon energy was set at the values corresponding to the $2s \rightarrow 4p$ and $5p$ absorption maxima with the aid of total ion yield measurements. The total ion yield spectrum depicted in Fig. 1 was measured with entrance and exit slits set at 33 and 30 μm, respectively, corresponding to a photon bandwith of 75 meV. Both the resonant Auger and photoelectron spectra were measured with a photon bandwidth of about 80 meV. The pass energies of the electron energy analyzers were set at 5 eV, which resulted in kinetic energy resolutions of 100–150 meV depending on the analyzer. The binding energy scale was calibrated according to the Ar $2p$ photoelectron lines, whose binding energies are known within an accuracy of ± 0.01 eV [18]. The positions of the Ar $2p$ photoelectron lines were checked between resonant Auger measurements in order to detect possible changes in the energy of the incoming photon beam. The argon $2p$ photoelectron satellite spectrum was also measured at a photon energy about 10 eV below the resonant excitations, where the intensity in the binding energy region of interest is given by direct $2p$ photoionization.

The method for calibration of the detection efficiencies of the ten analyzers was already presented in [19]. In contrast to that study, in the present case the transmission of the analyzers can be expected to vary also as a function of kinetic energy. Therefore the Ar $3s$ photoelectron line, the β of which is 2, was measured at several photon energies to calibrate the relative intensities of the different analyzers in the kinetic energy region of interest. The transmission-corrected experimental photoelectron spectrum (off resonance) is presented in Fig. 2(a) whereas Figs. 2(b) and 2(c) depict the electron spectra measured at the $2s \rightarrow 4p$ and $2s \rightarrow 5p$ excitations, respectively.

The energies and intensities of all detection-sensitivity and relative-transmission corrected electron spectra, including photon-flux normalized total ion yield spectra, were determined with a least-squares fitting program [20]. The line shapes in the fits of total ion and photoelectron spectra were produced using Voigt functions. The Lorentzian component of the Voigt function described the natural width of the final state, whereas the Gaussian component represented the distributions of the photon bandwidth and, in the case of the photoelectron spectra, analyzer broadening. The line profiles of the resonant Auger lines were also chosen to be Voigt functions. The actual line shape of the resonant Auger line is not exactly a Voigt function, but the profile chosen reproduced the experimental lines very well. The Lorentzian final state broadening for all photoelectron and resonant Auger lines was estimated to be 118 meV, the same as found for the $2p^{-1}$ states in a recent study by Jurvansuu *et al.* [21].

III. CALCULATIONS

The amplitude of a resonant Auger line can be calculated following the time-independent scattering formalism (see [22] and references therein). Formally, the amplitude A_F can be presented as

$$A_F=\langle[f,f']\phi\varepsilon|V|o\rangle + \sum_{[i]} \int d\tau \frac{\langle[f,f']\phi\varepsilon|H-E_F|[i]\tau\rangle\langle[i]\tau|V|o\rangle}{E_F-E\tau+i\Gamma_{[i]}/2}. \tag{3.1}$$

The first term represents the amplitude for a direct transition from the ground state $|o\rangle$ to the final state $|[f,f']\phi\varepsilon\rangle$ with holes in the orbitals f and f', one electron excited to the orbital ϕ and another to the continuum ε. The second term is due to the contribution following resonant excitations. The integration over τ includes implicit summations over bound states. The matrix elements for the first term of Eq. (3.1) were calculated in the case of transitions into the $2p^{-1}3p^{-1}np$ states as

$$\langle[f,f']\phi\varepsilon|V|o\rangle=\epsilon_{ph}\langle 2p|r|\epsilon d\rangle c(2p^{-1}\epsilon d\,{}^1P) \times\langle 3p_o|np\rangle c(3p^{-1}4p\,{}^1S). \tag{3.2}$$

In Eq. (3.2) the subscript o indicates the ground-state wave function and each c is the mixing coefficient of the LS basis states in the intermediate coupling scheme. The notation ϵ_{ph} refers to the fact that energy dependence is included in the calculations. Initial calculations showed that ionization through the d continuum electron is approximately 31 times more probable than the ionization through the s continuum, therefore the actual calculations were performed using the d continuum electron only.

In the analysis of the $2p$ shake-up spectrum, energy calculations performed included the $2p^{-1}3p^{-1}np$, $2p^{-1}3p^{-1}ns$ ($n=4,5$), and $2p^{-1}3p^{-1}md$ ($m=3,4$) electron configurations. In general, the intensities of conjugate shake-up satellites are considerable only at the corresponding thresholds and decrease rapidly as the photon energy increases (see Ref. [23] and references therein). However, the $2p^{-1}3p^{-1}ns$ and $2p^{-1}3p^{-1}md$ conjugate shake-up satellites seem to produce some intensity in the kinetic energy region studied and therefore the configurations are included in the energy calculations. The direct photoionization channel of the satellite states was considered to have a constant cross section in the energy region of the measurements performed.

In the calculations concerning the interference effect, the Auger decay matrix elements, $\langle[f,f']\phi\varepsilon|H-E_F|[i]\tau\rangle$ in Eq. (3.1), were reduced to include transitions only to final ionic states with the same total angular momentum that could be populated via direct photoionization, i.e., ionic states that have $J=1/2$ or 3/2. The intensity to final ionic states with J higher than 3/2 was also added to the theoretical spectrum, but without interference effects. The resonant Auger decay was calculated using s,d, and g continuum electrons. The g continuum had no effect on the intensity distribution but the considerable intensity produced by the s continuum was added as noninterfering intensity. The relative intensities of the $2s^{-1}4p\rightarrow 2p^{-1}3p^{-1}5p$ shake-up transitions were calculated using the overlap integrals $\langle 4p_i|4p_f\rangle$ and $\langle 4p_i|5p_f\rangle$. The subscripts i and f indicate the intermediate and final states, respectively.

The dipole and Auger decay matrix elements, shake-up integrals, and eigenfunctions for the resonant and final states were calculated using the Hartree-Fock method with relativistic corrections [24]. The Slater and Coulomb integrals were scaled down by a factor of 0.85, the value written in the code. The scaling, which compresses the energy spread, is widely used to approximate configuration interaction effects (see, e.g., Ref. [25] and references therein). The continuum orbitals were generated in the configuration-average potentials of the $2p^{-1}3p^{-1}4p$ configuration. The continuum energy was calculated as a difference between the configuration average energies of the intermediate and final states.

Theoretical binding energies are presented in Fig. 3(a). Figure 3(b) presents the calculated Ar $2p$ photoelectron shake-up satellite spectrum and its components whereas Fig. 3(d) presents the theoretical resonant Auger spectrum without interference effects. Figure 3(c) depicts the resulting spectra when interference effects between the direct and resonant channels are either included or omitted.

IV. DISCUSSION

A. Ar $2p$ photoelectron satellites

The Ar $2p$ photoelectron satellite spectrum of Fig. 2(a), measured in the kinetic energy region of the $2p^{-1}3p^{-1}4p$ states, also includes some $2p^{-1}3p^{-1}5p$ states and some $2p^{-1}3p^{-1}(ns,nd)$ conjugated satellite states. As the measurement was done well below the excitation energy of the first $2s$ resonance state, the intensity distribution of the $2p^{-1}3p^{-1}np$ ($n=4,5$) states provides a reference to detect the effects related to the resonant Auger channels.

The experimental Ar $2p$ photoelectron shake-up satellite spectrum has been interpreted earlier [6] to contain states belonging mostly to the $2p^{-1}3p^{-1}np$ ($n=4,5$) electron configurations but there were no calculations for the intensity distribution of the spectrum. Our calculations reproduce quite well the experimental spectrum as can be seen by comparing Figs. 2(a) and 3(b). In particular, energy splittings are reproduced very well. The strongest components in the experimental photoelectron spectrum [see Fig. 2(a)] can be identified with the aid of the calculations. The assignments and binding energies of the peaks are given in Table I. Notations used in the table refer to the parent term in the $2p^{-1}3p^{-1}(^{2S+1}L_J)np$ configuration. At around 275 eV binding energy, four peaks ($8-11$) were used in the fit although theoretically there should be only two $2p^{-1}3p^{-1}np$ ($n=4,5$) states. However, energy calculations [see Fig. 3(a)] suggest that those additional peaks could be assigned as $2p^{-1}3p^{-1}nd$ states. The small structures around $270-267$ eV in the photoelectron spectrum of Fig. 2(a) were identified as $2p^{-1}3p^{-1}3d$ and $2p^{-1}3p^{-1}4s$ conjugate shake-up satellites.

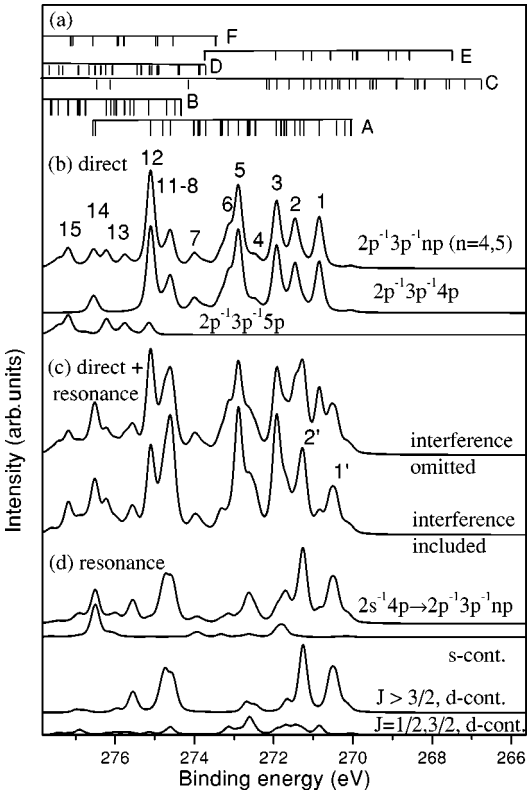

FIG. 3. (a) Theoretical binding energies of the Ar $2p$ shake-up satellites. Labels A to F refer to $2p^{-1}3p^{-1}4p$, $2p^{-1}3p^{-1}5p$, $2p^{-1}3p^{-1}3d$, $2p^{-1}3p^{-1}4d$, $2p^{-1}3p^{-1}4s$, and $2p^{-1}3p^{-1}5s$ configurations, respectively. (b) Theoretical Ar $2p$ photoelectron shake-up satellite spectrum. The curves show the intensity to the $2p^{-1}3p^{-1}4p$ and $2p^{-1}3p^{-1}5p$ states as well as their sum spectrum.(c) Theoretical electron spectrum of Ar at the $2s\rightarrow 4p$ excitation energy with and without interference effects. (d) Theoretical resonant Auger spectrum of Ar at $2s\rightarrow 4p$ excitation energy without interference effects. The lowermost spectrum presents transitions to final ionic states with $J=1/2,3/2$ and d continuum. The following two spectra present calculated intensity to final ionic states with $J \geqslant 3/2$ and results from s continuum calculations. The uppermost spectrum is the sum spectrum of the three individual components. The theoretical binding energies are shifted by -0.14 eV so that the energy scale coincides with experiment at the position of peak No. 1 (see Fig. 2).

The experimental angular distribution parameters β were determined for all fitted components in the spectrum in order to detect possible changes when the resonant channel populates the same states. The β values of the strongest components in the experimental photoelectron shake-up spectrum are presented in Table I. The values obtained are similar to or slightly larger than those given for the main line ($\beta \approx 0.5$–0.8) in this kinetic energy range by Lindle *et al.* [26].

B. Total ion yield

The excitation energies for the $2s\rightarrow 4p,5p$ resonances were extracted to be 323.6 ± 0.2 eV and 324.9 ± 0.3 eV, respectively using the total ion yield measurement. The very large inherent width of the Ar $2s^{-1}$ state made the analysis of the excitation energy in the case of the Ar $2s\rightarrow 5p$ quite difficult. The experimental energy difference between the $2s\rightarrow 4p$ and $2s\rightarrow 5p$ excitations, 1.3 ± 0.1 eV, is identical with the theoretical value of 1.34 eV reported in Ref. [14]. The values extracted for the natural widths of the $2s^{-1}np$ ($n=4,5$) resonant states, 2.0(2) eV, are slightly smaller than the width reported for the $2s^{-1}$ state by Glans *et al.* [9], 2.25(5) eV. The natural widths of the $2s^{-1}np$ states are bigger than the energy difference between them, thus allowing also interresonance interference effects to occur. The theoretical value for the lifetime width of the Ar $2s^{-1}4p$ state obtained from the calculations, 2.1 eV, is in very good agreement with the experimental result. According to the data presented in Fig. 1, the $2s\rightarrow 5p$ excitation strength is about 0.34 of the strength of the $2s\rightarrow 4p$ excitation. The calculation performed for the photoexcitation strengths gave a slightly smaller value of 0.31, which still compares favourably with the experimental value.

TABLE I. Experimental binding energies of the most prominent peaks in the Ar $2p$ shake-up spectrum. Line numbers refer to Fig. 2(a). The values of the angular distribution parameters β obtained from the photoelectron spectrum ($h\nu=310$ eV) are presented in comparison with those from the electron spectrum measured at the $2s^{-1}4p$ resonance.

No.	E_B (eV)	Assignment	Photoelectron β	$2s\rightarrow 4p$ resonance β
1	270.9(2)	$(^3D)4p$	0.70(11)	0.93(14)
2	271.4(2)	$(^3D)4p$	$-0.2(4)$	0.45(6)
3	271.8(2)	$(^3S)4p$	0.65(14)	0.22(12)
4	272.6(2)	$(^3P)4p$	0.52(11)	0.29(15)
5	273.0(2)	$(^3D)4p$	1.85(10)	2.0(3)
6	273.2(2)	$(^3D)4p$	0.43(7)	0.67(12)
7	273.7(2)	$(^3P)4p$	1.3(5)	1.3(3)
8	274.5(2)	$(^1D)4p$	1.0(2)	1.3(2)
9	274.7(2)	$(^1D)4p$	0.79(12)	0.3(1)
10	274.9(2)	$(^1D)4p$	0.95(10)	1.1(4)
11	275.1(2)	$(^1D)4p$	0.8(2)	0.3(3)
12	275.5(2)	$(^1D)4p$	0.6(2)	0.6(3)
13	276.4(2)	$(^3S)5p$	1.1(3)	0.8(2)
14	276.6(2)	$(^1S)4p$	1.1(4)	0.75(6)
15	277.2(2)	$(^3D)5p$	1.2(4)	0.79(10)
1'	270.5(2)	$(^3D)4p$		$-0.70(6)$
2'	271.3(2)	$(^3D)4p$		$-0.3(2)$

C. Resonant Auger decay

In order to make a comparison between the on and off resonance spectra easier, we depict in Fig. 4 experimental and theoretical photoelectron shake-up and resonant Auger spectra above each other using the same labels as in Fig. 2. The variation of the line intensities due to the resonant Auger channel is clearly seen by comparing the two experimental spectra of Fig. 4(a). The experimental angular distribution parameters β were determined for all fitted components in the $2s^{-1}4p\rightarrow 2p^{-1}3p^{-1}np$ resonant Auger spectrum. The β values of the strongest components are presented in Table I in comparison with the corresponding values of the photo-

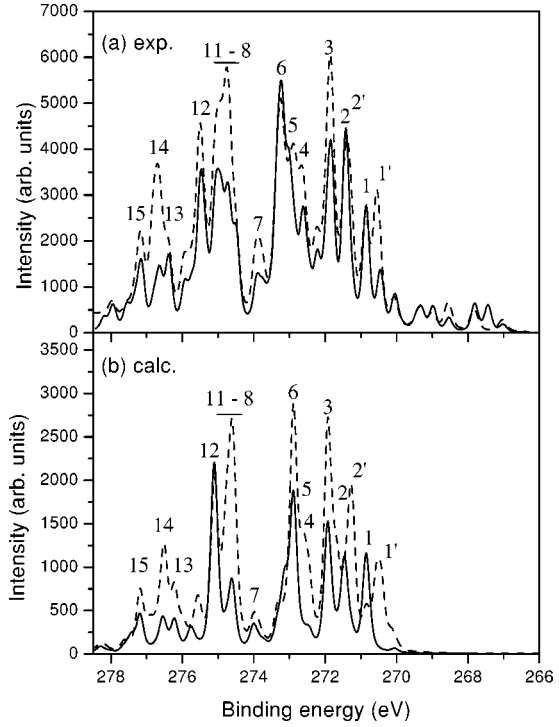

FIG. 4. (a) Fits for the experimental Ar $2p$ photoelectron shake-up satellite spectrum measured below the first $2s$ excitation energy (solid line) and for the electron spectrum taken at the $2s \rightarrow 4p$ excitation energy (dashed line).(b) Theoretical photoelectron spectrum of Ar below the first $2s$ excitation energy (solid line) and theoretical electron spectrum of Ar at the $2s \rightarrow 4p$ excitation energy based on the one-step calculations (dashed line).

electron spectrum. The effect of the resonant decay channel is clearly considerable especially in the states which are strongly populated via resonant Auger decay, e.g., lines 3 and 9 [see Fig. 4(a)].

The $2s^{-1}4p$ state also decays to final ionic states with $J>3/2$ which are not populated via photoionization. The most prominent of such transitions gives rise to the peak $1'$ in Figs. 3(c) and 4(b). The peak is also clearly visible in the experimental spectrum. As pointed out in Sec. III, the resonant Auger decay with the s continuum gives additional intensity to states with $J=1/2,3/2$, i.e., to states which are populated via photoionization to the d continuum. The effect of this additional decay channel is most distinctly seen as a strong enhancement in intensity of the $(^1S)4p$ line [label 14 in Figs. 3(c), 2(b), and 4(b)].

The differences between the calculations performed with or without interference effects are shown in Fig. 3(c). Although the differences are small they cannot be neglected. The best indication of a need to account for the interference effects can be seen in the vicinity of the structures labeled with 1 and 2. The calculations neglecting the interference effects produce more intensity in peaks whose experimental intensities remain constant or even decrease in going from off resonance to on resonance.

Most of the differences between the two spectra in Fig. 4(a) can be explained with the aid of the theoretical photoelectron and resonant Auger spectra depicted in Fig. 4(b). Particularly, the theoretical resonant Auger spectrum based on the one-step calculations predicts very well the intensity distribution near lines 1 and 2. In the theoretical spectrum [Fig. 4(b)], the intensity of line 1 decreases far more than in the experimental spectrum but the direction of the change is correct. Theoretically, a resonant Auger line ($J>3/2$), labeled as $2'$, appears just beside peak 2, thus increasing the intensity in this region, but it should also be noted that line 2 itself is slightly decreasing. This effect is also seen in the experimental resonant Auger spectrum of Fig. 4(a) but the effect is not so pronounced due to a slightly smaller experimental energy difference between peaks 2 and $2'$. In the region of lines 4–7 both calculations seem to reproduce the experimental spectrum fairly well but in the region of lines 8–12 the one-step calculations reproduce the intensity ratios of the lines much better than calculations neglecting interference as can be seen by comparing Figs. 3(c) and 4(a).

The $2s^{-1}5p \rightarrow 2p^{-1}3p^{-1}np$ resonant Auger spectrum [see Fig. 2(c)] was measured using a photon energy slightly higher (0.2 eV) than that of the maximum of the $2s \rightarrow 5p$ excitation. As is seen from Fig. 1, the $2s \rightarrow 4p$ and $5p$ excitations are overlapping and at the photon energy used in the mesurement the $2s \rightarrow 4p$ excitation is almost as strong as the $2s \rightarrow 5p$ excitation. Therefore the similarity of the two experimental resonant Auger spectra is not unexpected. The effect of the resonant Auger decay is clearly visible. One step calculations were not performed for the case of $2s \rightarrow 5p$ excitation. Further work is needed to theoretically account for the existence of many overlapping final states as well as two almost equally populated intermediate states decaying to the same final ionic states.

V. CONCLUSIONS

The excitation energies and the linewidths of the Ar $2s^{-1}np$ ($n=4,5$) states were determined from the high-resolution total ion yield spectrum measured below the $2s$ ionization threshold. The Ar $2p$ photoionization shake-up satellite structures were resolved in the region of the $2p^{-1}3p^{-1}np$ shake-up states. The theoretical calculations predicted the structures in the experimental spectrum reasonably well. Even when the $2p^{-1}3p^{-1}np$ satellite states were populated via both direct and resonant channels, the one-step calculations could explain most of the intensity changes. However, the results of the calculations clearly show a need for more elaborate methods when there are two interfering channels.

ACKNOWLEDGMENTS

The staff of ELETTRA are acknowledged for assistance during the measurements. This work was supported by the European Union (Project No. ERB FMGE CT95 0022-A.N°1) and the Research Council for the Natural Sciences of the Finnish Academy.

[1] R. Camilloni, M. Žitnik, C. Comicioli, K.C. Prince, M. Zacchigna, C. Crotti, C. Ottaviani, C. Quaresima, P. Perfetti, and G. Stefani, Phys. Rev. Lett. **77**, 2646 (1996).
[2] R.R.T. Marinho, O. Björneholm, S.L. Sorensen, I. Hjelte, S. Sundin, M. Bässler, S. Svensson, and A. Naves de Brito, Phys. Rev. A **63**, 032514 (2001).
[3] D.P. Spears, H.J. Fischbek, and T.A. Carlson, Phys. Rev. A **9**, 1603 (1974).
[4] K.G. Dyall, F.P. Larkins, K.D. Bomden, and T.D. Thomas, J. Phys. B **14**, 2551 (1981).
[5] D.J. Bristow, J.S. Tse, and G.M. Bancroft, Phys. Rev. A **25**, 1 (1982).
[6] B. Eriksson, S. Svensson, N. Mårtensson, and U. Gelius, J. Phys. B **21**, 1371 (1988).
[7] L. Avaldi, G. Dawber, R. Camilloni, G.C. King, M. Roper, M.R.F. Siggel, G. Stefani, and M. Žitnik, J. Phys. B **27**, 3953 (1994).
[8] T. Hayaishi, E. Murakami, Y. Morioka, H. Aksela, S. Aksela, E. Shigemasa, and A. Yagishita, J. Phys. B **25**, 4119 (1992).
[9] P. Glans, R.E. La Villa, M. Ohno, S. Svensson, G. Bray, N. Wassdahl, and J. Nordgren, Phys. Rev. A **47**, 1539 (1992).
[10] W. Mehlhorn, Z. Phys. **208**, 1 (1968).
[11] T. Kylli, J. Karvonen, H. Aksela, A. Kivimäki, S. Aksela, R. Camilloni, L. Avaldi, M. Coreno, M. de Simone, R. Richter, K.C. Prince, and S. Stranges, Phys. Rev. A **59**, 4071 (1999).
[12] P. Lablanquie, F. Penent, R.I. Hall, H. Kjeldsen, J.H.D. Eland, A. Muehleisen, P. Pelicon, Ž. Šmit, M. Žitnik, and F. Koike, Phys. Rev. Lett. **84**, 47 (2000).
[13] B.S. Itchkawitz, B. Kempgens, H.M. Köppe, J. Feldhaus, A.M. Bradshaw, and W.B. Peatman, Rev. Sci. Instrum. **66**, 1531 (1995).
[14] A.N. Khoperskii and V.A. Yavna, Opt. Spektrosk. **82**, 5 (1997).
[15] J. Karvonen, A. Kivimäki, H. Aksela, S. Aksela, R. Camilloni, L. Avaldi, M. Coreno, M. de Simone, and K.C. Prince, Phys. Rev. A **59**, 315 (1999).
[16] K.C. Prince, R.R. Blyth, R. Delaunay, M. Žitnik, J. Krempasky, J. Slezak, R. Camilloni, L. Avaldi, M. Coreno, G. Stefani, C. Furlani, M. De Simone, and S. Stranges, J. Synchrotron Radiat. **5**, 565 (1998).
[17] R.R. Blyth, R. Delaunay, M. Žitnik, J. Krempasky, R. Krempaska, J. Slezak, K.C. Prince, R. Richter, M. Vondracek, R. Camilloni, L. Avaldi, M. Coreno, G. Stefani, C. Furlani, M. de Simone, S. Stranges, and M.-Y. Adam, J. Electron Spectrosc. Relat. Phenom. **101-103**, 959 (1999).
[18] L. Petterson, J. Nordgren, L. Selander, C. Nordling, K. Siegbahn, and H. Ågren, J. Electron Spectrosc. Relat. Phenom. **17**, 29 (1982).
[19] R. Sankari, A. Kivimäki, M. Huttula, H. Aksela, S. Aksela, M. Coreno, G. Turri, R. Camilloni, M. de Simone, and K.C. Prince, Phys. Rev. A **63**, 032715 (2001).
[20] H.M. Köppe, A.L.D. Kilcoyne, J. Feldhaus, and A.M. Bradshaw, J. Electron Spectrosc. Relat. Phenom. **75**, 97 (1995).
[21] M. Jurvansuu, A. Kivimäki, and S. Aksela, Phys. Rev. A **64**, 012502 (2001).
[22] G.B. Armen, H. Aksela, T. Åberg, and S. Aksela, J. Phys. B **33**, R49 (2000).
[23] A. Ausmees, S.J. Osborne, S. Svensson, A. Naves de Brito, O.-P. Sairanen, A. Kivimäki, E. Nõmmiste, H. Aksela, and S. Aksela, Phys. Rev. A **52**, 2943 (1995).
[24] R.D. Cowan, *The Theory of Atomic Structure and Spectra* (University of California Press, Berkeley, 1981).
[25] A. von dem Borne, R.L. Johnson, B. Sonntag, M. Talkenberg, A. Verweyen, Ph. Wernet, J. Schulz, K. Tiedtke, Ch. Gerth, B. Obst, P. Zimmermann, and J.E. Hansen, Phys. Rev. A **62**, 052703 (2000).
[26] D.W. Lindle, L.J. Medhurst, T.A. Ferrett, P.A. Heimann, M.N. Piancastelli, S.H. Liu, D.A. Shirley, T.A. Carlson, P.C. Deshmukh, G. Nasreen, and S.T. Manson, Phys. Rev. A **38**, 2371 (1988).